

## Field Paradigm for 3D Medical Imaging

*"Nothing is invisible, not even our thoughts!"*

**Dr. Murali Subbarao, Ph.D.**

Professor of Electrical and Computer Engineering, Stony Brook, New York, USA.

*murali@fieldparadigm.com*, [www.fieldparadigm.com](http://www.fieldparadigm.com),

### **Abstract:**

Measurement and analysis of emission fields (i) at points distributed in a full 3D volume space instead of a 2D surface, and (ii) along different directions when necessary, provides additional new information that has been overlooked so far. This technology can lead to dramatic improvements in the safety, accuracy, and speed, of 3D medical imaging systems like SPECT/PET, MRI, ultra low-field MRI, and MEG. Expediting the application of this technology through further innovations and development will greatly benefit the public. Disproving this technology, in case its mathematical basis presented here is incorrect, would be easy and quick for the experts, and they are invited to try it as a service to the public.

### **1. Field Paradigm**

*Field Paradigm* (FP) is a novel theoretical and computational framework for 3D medical imaging. It is based on the measurement and analysis of emission fields in a full 3D volume space around a target object, including measurements at different radial distances and possibly along different directions and apertures, at each point. Analysis of flux field intensity and its directional components in a 3D volume space reveals the 3D spatial density distribution of field emitting sources. This is unlike conventional imaging methods and devices that limit measurements to points in a subspace or a cross-section such as a 2D surface at a nearly constant radial distance from the target object. In some cases, such measurement is equivalent to measuring only one (usually) dominant component of the 3D flux field that is normal to the 2D surface and ignoring information in other components. Researchers in the past have overlooked additional new information provided by measurements at different radial distances and directions. They assumed implicitly and incorrectly, that such measurements would only provide redundant or insignificant information. It is a mathematical certainty that this assumption is wrong and it can be easily proved to be so. In this sense *Field Paradigm* is *information-efficient*-- it exploits all available information that is imageable and useful for 3D image reconstruction. The amount of information imaged and used in *Field Paradigm* is typically 2 to 10 times more than that measured and used by conventional

methods; this is a mathematical certainty and it results in tremendous advantages. *Field paradigm* has been verified through rudimentary computer simulations in a few simple cases.

In comparison with current techniques, *Field Paradigm* provides 3D medical imaging methods and devices that are much safer (e.g. lower radiation in nuclear medicine), much faster (i.e. shorter image scanning time), and more accurate (higher spatial, temporal, and brightness/contrast resolution) resulting in significant improvement in the correct diagnosis of patients. The optimal information-efficiency of *Field Paradigm* may prove crucial in limited view-field tomography, i.e. applications where imaging field of view is very localized or limited by the shape of the target object.

*Field Image Tomography* (FIT) deals with the practical design of imaging devices, measurement techniques, and computational algorithms, for 3D imaging of objects based on *Field Paradigm*. Detailed descriptions of the application of FIT to many methods and apparatuses for 3D medical imaging are presented in several patent applications filed by this author during 2009-2011 [1-6].

### **2. Applications**

*Field Paradigm* is expected to provide dramatic improvements in SPECT/PET (Single-Photon Emission Computed Tomography / Positron Emission Tomography) [1], MRI (Magnetic Resonance Imaging) [2], ultra low-field MRI [4], and MEG/MCG (Magnetoencephalography/Magnetocardiography) [3]. According to current estimates, radiation dosage in SPECT [1] can be reduced by over 70%, scanning time in MRI can be reduced by over 70% [2], and in MEG [3], *Field Paradigm* provides a closed-form solution to the problem of 3D image reconstruction which was thought to be under-constrained and therefore unsolvable. *Field paradigm* also suggests entirely new imaging modalities such as the Magnetic Density Imaging (MDI) [4] which could be a faster, cheaper, and safer substitute for MRI. MDI could be combined with MRI or ultra low-field MRI for trade-off in accuracy, speed, and cost.

Field Paradigm is also relevant to X-ray Computed Tomography (CT) [5], Ultrasound (US) CT, and Diffusion Optical Tomography (DOT). In these cases, according to current estimates, Field Paradigm offers a small improvement but not significant. The improvements derive from measuring both the direction and strength/intensity of scattered rays in a 3D volume space at each point and extracting the additional information therein. Details of these applications are provided in [5]. In Magnetic Resonance Spectroscopy (MRS), cancerous tumors are detected and localized based on the chemical composition of tumors. MRS imaging time could be reduced by 50% or more using devices based on Field Paradigm.

### 3. Field Image Principle

Field Paradigm is based on the *Field Image Principle (FIP)* that *the 3D spatial density distribution of a field emission source is uniquely determined by the flux density distribution of the field produced by the source in a 3D volume space around the source, and vice versa*. This principle has not been realized, recognized, or exploited in the past in 3D medical imaging. It can be understood intuitively by recognizing that field intensity (or flux density) varies with radial distance and direction from its source elements. The pattern or structure of 3D field intensity distribution can uniquely determine the location and distribution of its source elements. Consequently, in principle, there is no need for separate spatial encoding schemes such as frequency and phase encoding used in conventional MRI. Also, in principle, severe mechanical/electronic aperture collimation used in conventional SPECT/PET is not required. In practice, Field Paradigm can be combined with current techniques for optimal trade-offs between speed, safety, accuracy, and cost. Imaging all that is imageable and useful, and employing information-efficient algorithms for 3D image reconstruction, are the two critical elements that facilitate optimal trade-offs in Field Paradigm.

### 4. Current SPECT methods and Field Paradigm

Current 3D medical imaging techniques such as SPECT do not measure or exploit all available information. For example, just one photon out of 5,000 information carrying (non-scattered) photons may be measured in a typical SPECT machine. The information in other photons are wasted by blocking them through mechanical collimation. This is due to the inherent limitation of the basic theory underlying current methods. The theory underlying current methods can deal with photons coming from only one direction instead of all possible directions. Field paradigm is free from this limitation. In summary, much useful information is ignored and therefore current techniques are inefficient, harmful, less accurate, slow, and suboptimal in the diagnosis of

patients. They rely on measurement of (attenuated) *line-integrals* or *projections of field source density functions*. Measurements are typically restricted to points on a planar surface at different angular positions and at a nearly constant radial distance (see Fig. 1). Further, measurements are usually limited to be along a *single direction of view* (radial direction).

Field Paradigm exploits information in the field intensity (flux density) distribution in a 3D volume space (see Fig. 2) around the source. It measures and uses all available information, and consequently offers advantages of being safer, faster, and more accurate. Instead of only line integrals of mere field source density, (attenuated) *volume integrals* of actual *field intensity* or *flux density* are measured. Further, measurements are made at a set of non-degenerate points that are distributed in a *3D volume space* instead of on a roughly 2D surface such as a cylindrical surface. In addition, at each point, measurement of field flux density may be made along more than one direction, e.g. 3 mutually perpendicular directions, instead of just one direction such as the radial direction. This measured data, unlike current approaches that ignore much useful information, captures all the information that is useful in 3D image reconstruction.

One result of an improved SPECT based on Field Paradigm is that such SPECT machines could be used in Positron Emission Tomography (PET). Conventional PET machines are very expensive while the new SPECT machines that can replace PET machines will be very inexpensive.

### 5. Significance

Perhaps the most important consequence of Field Paradigm may be to avoid harmful X-ray radiation in the imaging of soft-tissue parts such as breast, heart, and abdomen. Field Paradigm could facilitate the substitution of X-ray computed tomography (CT) with equally fast and accurate but harmless MRI/MDI. X-rays are ionizing radiation and may cause cancer in patients but MRI/MDI is completely safe. Another important consequence could be low-cost and high-resolution ultra low-field MRI/MDI at video rate where the magnetic field strength is comparable to that of the earth. In this case, minimally invasive surgery could be performed under continuous tomographic video monitoring and guidance based on ultra low-field MRI/MDI in real-time.

Field paradigm provides a new closed-form solution to MEG. This problem was thought to be under-constrained and unsolvable because some essential and available information was not recognized, measured, or used. This information is the magnetic field variation at different radial distances and directions. Successful application of Field Paradigm

to MEG could result in fundamental advances in the diagnosis of brain illnesses and in understanding the functional and thought processes in the brain. Advances are likely in devices for recording and stimulating/inducing electrical current patterns corresponding to thought processes in the brain based on the new MEG machines. They could provide a direct but non-invasive method for human-computer two-way communication and interaction.

Field paradigm may also advance limited field of view and localized imaging for medical diagnosis due its inherent information-efficiency.

**6. Conclusion**

*Field Paradigm* is based on a simple and natural theory that holds significant promise in 3D medical imaging. It is surprising that it was not realized earlier. It could provide a new generation of machines for fast and safe MRI that could replace harmful X-ray CT, fast and ultra low-field MRI/MDI/MRS, low radiation SPECT/PET, and high-resolution and faster MEG/MCG. It could usher in a new era in safer, faster, and more accurate 3D medical imaging. There are no significant disadvantages associated with Field Paradigm. In light of this paradigm, other imaging devices and techniques in medical and other areas should be re-examined and evaluated for possible improvements, and the possibility of novel imaging modalities (e.g. MDI) should be explored.

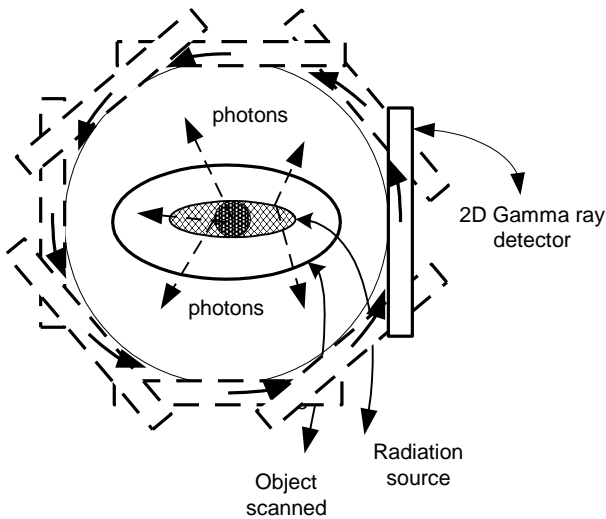


Fig. 1. Conventional SPECT apparatus. One or more 2D planar gamma detectors are rotated around the object of study in a circle of constant radius. Images are captured at regular intervals of 1 to 5 degrees apart. Volume space covered by the detector is very thin along the radial direction. Collimator field of view is small (around 3 degrees) along the radial direction and only photons in this narrow field of view (that is just about 1 out of 5,000 non-scattered photons) are measured while other are ignored.

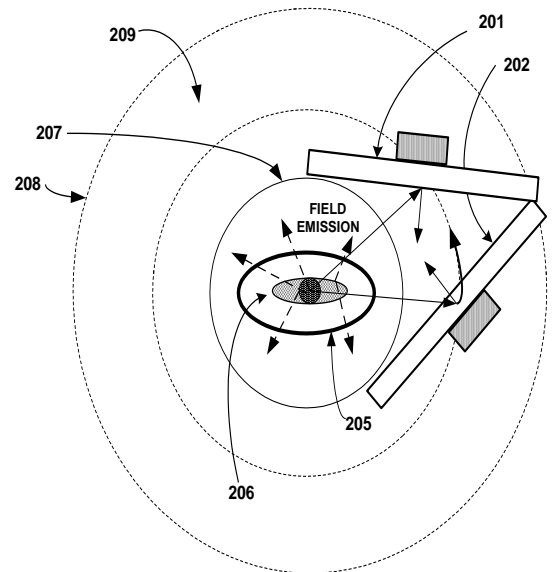


Fig. 2 Legend:  
 201, 202: 2D Field flux density sensor array at +45 degrees and -45 degrees respectively.  
 205: Object with field source.  
 206: Field source distribution.  
 207/208: inner/outer boundary of volume space.  
 209: 3D volume space where field flux density is measured.

Fig.2. Apparatus for SPECT based on Field Paradigm. Two 2D planar array detectors that measure field flux density are at +45 degrees and -45 degrees to the radial direction. They rotate around the object of study containing field emission source. Field intensity images are captured at regular intervals of around 3 to 5 degrees. The detectors sweep a 3D volume space and measure emission field intensity in a 3D volume space that extends substantially along the radial direction. It also measures field flux density along two different directions of +45 degrees and -45 degrees. Each detector pixel can have a wide-angle field of view of 10 degrees or more. Therefore, about 10 times more information carrying photons are intercepted and measured compared to 3-degrees field of view (number of photons is proportional to the square of the angle of field of view).

**7. References**

**Patent Applications by M. Subbarao:**

1. SPECT, PET: US Patent No. 8,008,625 B2, issued on Aug. 30, 2011.
2. MRI: US Patent Application No. 12/658,001, Date 02/01/2010.
3. MEG and MCG : US Patent Application No. 12/924,959, Date 10/9/2010.
4. Low-field MRI, MDI: US Patent Appl. No. 12/927,653, Date 11/20/2010.
5. X-ray CT, US, DOT: Prov. Appl. For Patent , No. 61/337,973, filed 2/12/2010, and Feb. 2011.

**Appendix A. Proof of Field Paradigm**

Detailed proof of Field Paradigm can be found in the references listed earlier. A brief outline will be presented here.

Application of Field Paradigm to determine the 3D mass density distribution of the earth for mineral and oil exploration is summarized below. This is a very simple example compared to SPECT as it avoids many complications such as aperture geometry, attenuation, and scatter problems. Surprisingly, the simple method outlined here was not found in the literature searched by this author.

Let  $f(\mathbf{r})$  be the mass density of the earth at a 3D position vector  $\mathbf{r}$  and let  $\mathbf{g}(\mathbf{r}')$  be the gravitational force vector on a unit mass at position vector  $\mathbf{r}'$ . The gravitational forces on the unit mass due to the mass in each volume element of size  $dV$  in the earth are found. Then they are summed separately along 3 mutually perpendicular directions over the total volume  $V$  of the earth. This gives the integral equation (note: bold face letters denote 3D vectors):

$$\mathbf{g}(\mathbf{r}') = \int_V \mathbf{h}(\mathbf{r}' - \mathbf{r}) f(\mathbf{r}) dV$$

where, for some constant  $c$ ,

$$\mathbf{h}(\mathbf{r}' - \mathbf{r}) = c(\mathbf{r}' - \mathbf{r}) / |\mathbf{r}' - \mathbf{r}|^3.$$

This 3D convolution equation can be solved easily and efficiently in the 3D Fourier domain. Using subscripts to denote respective components and upper case letters to represent Fourier transforms, the solution is given by

$$\mathbf{F}(\mathbf{u}) = \mathbf{G}_x(\mathbf{u}) / \mathbf{H}_x(\mathbf{u}) = \mathbf{G}_y(\mathbf{u}) / \mathbf{H}_y(\mathbf{u}) = \mathbf{G}_z(\mathbf{u}) / \mathbf{H}_z(\mathbf{u}).$$

The equation above indicates that a solution is possible. Here  $\mathbf{g}(\mathbf{r}')$  has been measured in a 3D volume space, not a 2D surface. In the discrete version of this problem a linear system of equations is set up. It corresponds to the convolution integral seen earlier.  $\mathbf{g}(\mathbf{r}')$  is measured at a non-degenerate set of points  $\mathbf{r}'$  distributed in a 3D volume space instead of a 2D surface. In this case, the linear system of equations can be solved to obtain the 3D mass density distribution  $f(\mathbf{r})$ . This discrete version of the algorithm was implemented and tested using a simulation software for a small data set where the earth was modeled by a 5x5x5 voxel cube with randomly generated density values.

Another simple computer simulation related to SPECT was carried-out. It included pixels with 180-degree field-of-view, and without emission attenuation or scatter due to surrounding medium. The object was a planar 5x5 voxel slice. In this case, measurements at points on a circle (i.e. points at a constant radial distance) did not provide a solution or provided a

solution with a very bad condition number (unstable solution that can be thrown off wildly in the presence of noise). Measurement at the same number of points at different radial distances corresponding to the Field Paradigm provided stable solutions. More complicated simulations are being investigated.

**Epilogue**

A new approach to 3D medical imaging is presented here. It is potentially safer, more accurate, and faster, than the current approaches. It could greatly benefit all the patients of SPECT/PET, MRI, MEG, and perhaps other imaging modalities. It is now up to the experts, in the interest of the public, to disprove the new approach or improve it further for use in clinical practice.

A patent based on the new approach to SPECT/PET has been issued recently (US Patent No. 8,008,625, issue date 8/30/2011). Several other patents on MRI, ultra low-field MRI, and MEG are pending. It is a mathematical certainty that the new approach exploits more information, for example through a larger field of view in SPECT, than current approaches. The theory underlying the new approach is surprisingly simple and short which makes it easy and quick to prove/disprove.

If a new approach is invented in one area but has applications in several areas, then this wider application is usually recognized in a short period and exploited. Conversely, since the current new approach is novel in SPECT/PET imaging (according to my literature search and the US patent office), it is very likely that it is novel in other imaging modalities. In fact, the novelty of the current invention is easiest to verify in MEG area because, a search of the US patent database (in the "Abstract" section) for the keyword "Magentoencephalography" (MEG) turns up just 9 results (as of 10/4/2011).

As the new approach was unknown until this invention, clearly it has not been tested and shown to fail in practice. Current indications according to the theory and rudimentary computer simulation experiments are that it can work. However, as with most new inventions, further innovations and experimentation would be needed to develop actual products.

The next phase in commercializing this invention is to carry-out more realistic and thorough computer simulation experiments to test and evaluate the theory. Review of this technology by multiple independent experts is also an important step. These steps are to be followed by designing and developing actual prototypes and testing them. Comments and suggestions are welcome (send to [murali@fieldparadigm.com](mailto:murali@fieldparadigm.com)).

### Appendix B. Field Paradigm Theory

Field Paradigm will be described first for simple field sources of photons, electrostatic field, gravitational field, and magnetostatic fields. Later it will be extended to magnetic fields produced by electrical current patterns in MEG and to MDI.

Let (see Fig. 3)

$$\mathbf{r} = (x, y, z) \quad (1)$$

be a position vector, and  $f(\mathbf{r})$  be the spatial density distribution of an emission field source (e.g. radio-nuclide density in SPECT, and mass density in the case of gravitational fields), in a 3D volume space  $\mathbf{V}$ .  $f(\mathbf{r})$  is assumed to be zero outside the volume

$\mathbf{V}$  (i.e.  $f(\mathbf{r}) = 0$  for  $\mathbf{r} \notin \mathbf{V}$ ). Consider a volume element

$$dV = dV(\mathbf{r}) = dx dy dz = (\mathbf{i} \cdot d\mathbf{r})(\mathbf{j} \cdot d\mathbf{r})(\mathbf{k} \cdot d\mathbf{r}) \quad (2)$$

of the emission source at  $\mathbf{r}$ . Let

$$\mathbf{r}' = (x', y', z') \quad (3)$$

be another position vector where the field intensity is measured. Let  $\mathbf{h}(\mathbf{r}, \mathbf{r}')$  denote the Point Spread Function (PSF) of the field emission source. It specifies the field intensity or flux density measured at point  $\mathbf{r}'$  due to a unit field source at  $\mathbf{r}$ . In many applications, including SPECT/PET (ignoring attenuation in the medium), and mapping 3D mass density of earth,  $\mathbf{h}(\mathbf{r}, \mathbf{r}')$  has the form

$$\mathbf{h}(\mathbf{r}, \mathbf{r}') = \mathbf{h}(\mathbf{r}' - \mathbf{r}) = c (\mathbf{r}' - \mathbf{r}) / |\mathbf{r}' - \mathbf{r}|^3 \quad (4)$$

where  $c$  is a constant. For example, in vacuum,  $\mathbf{h}(\mathbf{r}, \mathbf{r}')$  for light or photon emitting sources,  $c = 1/(4\pi)$ . In the case of mapping 3D mass density of earth,  $-c = 6.67 \times 10^{-11} \text{ N m}^2/\text{kg}^2$  is the gravitational constant. In the case of dipole or multi-pole field sources,  $\mathbf{h}(\mathbf{r}, \mathbf{r}')$  has a little different form (see Appendix C) but the field paradigm is still applicable.

In component form, it can be written as

$$\mathbf{h}(\mathbf{r}, \mathbf{r}') = \mathbf{i} h_x(\mathbf{r}' - \mathbf{r}) + \mathbf{j} h_y(\mathbf{r}' - \mathbf{r}) + \mathbf{k} h_z(\mathbf{r}' - \mathbf{r}) \quad (5)$$

where,

$$h_x(\mathbf{r}' - \mathbf{r}) = c(x' - x) / |\mathbf{r}' - \mathbf{r}|^3 \quad (6)$$

$$h_y(\mathbf{r}' - \mathbf{r}) = c(y' - y) / |\mathbf{r}' - \mathbf{r}|^3 \quad (7)$$

$$h_z(\mathbf{r}' - \mathbf{r}) = c(z' - z) / |\mathbf{r}' - \mathbf{r}|^3 \quad (8)$$

$$|\mathbf{r}' - \mathbf{r}| = [(x' - x)^2 + (y' - y)^2 + (z' - z)^2]^{1/2} \quad (9)$$

Energy  $dE(\mathbf{r})$  emitted by a field source element of volume  $dV$  and density  $f(\mathbf{r})$  is given by

$$dE(\mathbf{r}) = f(\mathbf{r}) dV. \quad (10)$$

The field intensity  $d\mathbf{g}(\mathbf{r}')$  produced by this source element at the point  $\mathbf{r}'$  is given by

$$d\mathbf{g}(\mathbf{r}') = \mathbf{h}(\mathbf{r}, \mathbf{r}') dE(\mathbf{r}) = \mathbf{h}(\mathbf{r}, \mathbf{r}') f(\mathbf{r}) dV. \quad (11)$$

Therefore, using the *superposition principle* for the fields, the total measured field intensity  $\mathbf{g}(\mathbf{r}')$  at  $\mathbf{r}'$  due to all the field source elements within the volume space  $\mathbf{V}$  is obtained by summing or integrating the field intensity produced by each individual element of the field source in  $\mathbf{V}$  as

$$\mathbf{g}(\mathbf{r}') = \int_E d\mathbf{g}(\mathbf{r}') = \int_V \mathbf{h}(\mathbf{r}, \mathbf{r}') f(\mathbf{r}) dV \quad (12)$$

where

$$\mathbf{g}(\mathbf{r}') = \mathbf{i} g_x(\mathbf{r}') + \mathbf{j} g_y(\mathbf{r}') + \mathbf{k} g_z(\mathbf{r}'). \quad (13)$$

Note that this derivation is valid for those cases where the superposition principle holds. In particular, if diffraction and interference effects of waves need to be accounted for, then the derivation here will need to be modified and extended to those cases.

Given the field image

$$\mathbf{g}(\mathbf{r}') = \mathbf{i} g_x(\mathbf{r}') + \mathbf{j} g_y(\mathbf{r}') + \mathbf{k} g_z(\mathbf{r}') \quad (14)$$

measured at a *non-degenerate set  $\mathbf{R}'$  of points  $\mathbf{r}'$*  and given the PSF  $\mathbf{h}(\mathbf{r}, \mathbf{r}')$ , the integral equation

$$\mathbf{g}(\mathbf{r}') = \int_V \mathbf{h}(\mathbf{r}, \mathbf{r}') f(\mathbf{r}) dV \quad (15)$$

can be solved to obtain the desired unknown  $f(\mathbf{r})$ . In the discrete domain, a vector-matrix equation of the form

$$\mathbf{g} = \mathbf{H} \mathbf{f} + \mathbf{n} \quad (16)$$

can be written where  $\mathbf{g}$  denotes a column vector of measured data,  $\mathbf{H}$  denotes a system matrix related to the point spread function  $\mathbf{h}(\mathbf{r}, \mathbf{r}')$  of imaging apparatus,  $\mathbf{f}$  denotes a column vector of unknown field source distribution  $f(\mathbf{r})$  that needs to be solved for, and  $\mathbf{n}$  denotes noise in the measured data. The system matrix  $\mathbf{H}$  is affected by aperture, sensor geometry, and collimation. Attenuation and scattering due to propagation through target object can also be taken into account by modifying  $\mathbf{H}$ . A large system of linear equations is obtained. It can be solved using any one of many available techniques in the literature.

If  $\mathbf{h}(\mathbf{r}, \mathbf{r}')$  depends only on  $|\mathbf{r}' - \mathbf{r}|$ , as in the case of photon flux, gravity, electrostatics, magnetic dipoles, etc., then the integral equation becomes a convolution equation

$$\mathbf{g}(\mathbf{r}') = \int_V \mathbf{h}(\mathbf{r}' - \mathbf{r}) f(\mathbf{r}) dV \quad (17)$$

or, in component form

$$g_x(\mathbf{r}') = \int_V h_x(\mathbf{r}' - \mathbf{r}) f(\mathbf{r}) dV \quad (18)$$

$$g_y(\mathbf{r}') = \int_V h_y(\mathbf{r}' - \mathbf{r}) f(\mathbf{r}) dV \quad (19)$$

$$g_z(\mathbf{r}') = \int_V h_z(\mathbf{r}' - \mathbf{r}) f(\mathbf{r}) dV \quad (20)$$

which can be easily solved for  $f(\mathbf{r})$  in the Fourier domain. For example, representing respective Fourier transforms by upper case letters, we obtain

$$\mathbf{G}(\mathbf{u}) = \mathbf{i} G_x(\mathbf{u}) + \mathbf{j} G_y(\mathbf{u}) + \mathbf{k} G_z(\mathbf{u}) \quad (21)$$

$$\mathbf{H}(\mathbf{u}) = \mathbf{i} H_x(\mathbf{u}) + \mathbf{j} H_y(\mathbf{u}) + \mathbf{k} H_z(\mathbf{u}) \quad (22)$$

$$G_x(\mathbf{u}) = H_x(\mathbf{u}) F(\mathbf{u}) \quad (23)$$

$$G_y(\mathbf{u}) = H_y(\mathbf{u}) F(\mathbf{u}) \quad (24)$$

$$G_z(\mathbf{u}) = H_z(\mathbf{u}) F(\mathbf{u}) \quad (25)$$

$$F(\mathbf{u}) = G_x(\mathbf{u}) / H_x(\mathbf{u}) = G_y(\mathbf{u}) / H_y(\mathbf{u}) \\ = G_z(\mathbf{u}) / H_z(\mathbf{u}) \quad (26)$$

Note that, according to the three different solution expressions for  $F(\mathbf{u})$  above, in this case, in principle, measuring just one component of

$$\mathbf{g}(\mathbf{r}') = \mathbf{i} g_x(\mathbf{r}') + \mathbf{j} g_y(\mathbf{r}') + \mathbf{k} g_z(\mathbf{r}') \quad (27)$$

is sufficient to solve for  $f(\mathbf{r})$ . However, for best results, if only one component is measured, then it should be the radial component which will have a high magnitude and therefore a high signal to noise ratio. Tangential components will be generally weak and therefore signal-to-noise ratio for them will be low. Therefore the results will be more reliable for the radial components. A regularized inverse filter such as a Weiner filter or a spectral filter can be used for computing  $f(\mathbf{r})$  using the above equations.

A key observation here is that  $\mathbf{h}(\mathbf{r}, \mathbf{r}')$  plays an important role in providing a solution to the problem, and that the field image  $\mathbf{g}(\mathbf{r}')$  must be measured at a non-degenerate set  $\mathbf{R}'$  of points  $\mathbf{r}'$ . In particular, measurements must be made in a 3D volume space (e.g. Fig. 2) that extends substantially along the radial direction pointing away from the center of the field source. The measurement apparatus must specifically include a novel significant feature (which is lacking in current imaging devices) for making such measurements. Measurements must not be restricted (as in Fig. 1) to points on a surface such as a planar surface at different angular positions and at a nearly constant radial distance, which is usually the case in conventional SPECT imaging,

This theory can be extended to other fields such as electrical current patterns that generate magnetic field patterns in MEG and Magnetocardiography (MCG), as well as magnetic dipoles, and electrical/magnetic multipoles found in molecules. A summary is provided in Appendix C for MEG and for MDI in Appendix D.

The theory applicable to MEG is also applicable to MCG.

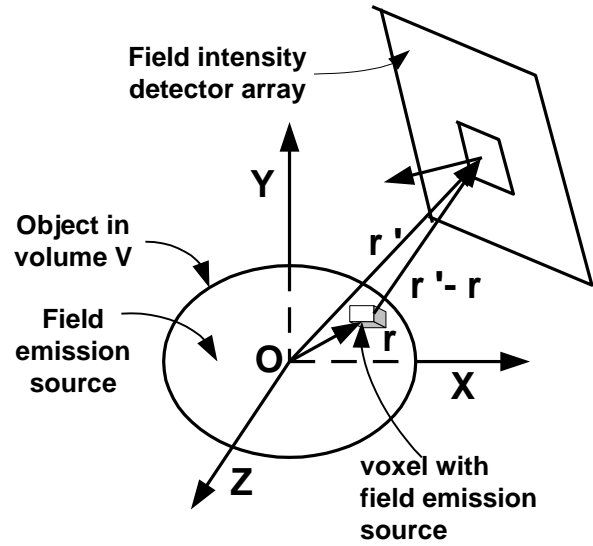


FIG. 3 Field emission source and measurement geometry.

### Appendix C: Magnetoencephalography (MEG)

Consider the brain to be made up of small cubic volume elements or voxels of dimensions  $dx$ ,  $dy$ ,  $dz$  along  $x$ ,  $y$ , and  $z$  axes, at each point

$$\mathbf{r} = \mathbf{i} x + \mathbf{j} y + \mathbf{k} z \quad (28)$$

in a volume space  $V$ . Let the electrical current density in each voxel be

$$\mathbf{J}(\mathbf{r}) = \mathbf{i} J_x(\mathbf{r}) + \mathbf{j} J_y(\mathbf{r}) + \mathbf{k} J_z(\mathbf{r}). \quad (29)$$

Let the measured magnetic field at a point

$$\mathbf{r}' = \mathbf{i} x' + \mathbf{j} y' + \mathbf{k} z' \quad (30)$$

be  $\mathbf{B}(\mathbf{r}')$ . The problem in MEG is, given  $\mathbf{B}(\mathbf{r}')$  measured at a large number of points  $\mathbf{r}'$  spread out along all dimensions in a 3D volume space around the brain, and measured along 3 mutually perpendicular directions, estimate  $\mathbf{J}(\mathbf{r})$ .

According to *Biot-Savart law*, the magnetific field  $d\mathbf{B}_1(\mathbf{r}')$  at  $\mathbf{r}'$  due to the  $x$ -axis component of current

$$I_x(\mathbf{r}) = J_x(\mathbf{r}) dA = J_x(\mathbf{r}) dy dz \quad (31)$$

$$\text{in a single voxel of size} \\ dV = dx dy dz \quad (32)$$

at  $\mathbf{r}$  is given by

$$d\mathbf{B}_1(\mathbf{r}') = (\mathbf{i} J_x(\mathbf{r}) dy dz dx) \times \left( c \frac{(\mathbf{r}' - \mathbf{r})}{|\mathbf{r}' - \mathbf{r}|^3} \right) \quad (33)$$

where constant  $c$  is

$$c = \mu_0 / (4\pi). \quad (34)$$

Therefore, the total magnetic field due to only the x-component of current is given by the volume integral

$$\mathbf{B}_1(\mathbf{r}') = c \int_V (\mathbf{i}J_x(\mathbf{r})) \times \frac{(\mathbf{r}' - \mathbf{r})}{|\mathbf{r}' - \mathbf{r}|^3} dV \quad (35)$$

Define

$$\mathbf{H}(\mathbf{r}' - \mathbf{r}) = c \frac{(\mathbf{r}' - \mathbf{r})}{|\mathbf{r}' - \mathbf{r}|^3} \quad (36)$$

Then we obtain

$$\mathbf{B}_1(\mathbf{r}') = \int_V (\mathbf{i}J_x(\mathbf{r})) \times \mathbf{H}(\mathbf{r}' - \mathbf{r}) dV \quad (37)$$

Eq. (37) above is a convolution-like expression. It can be solved easily in the Fourier domain if the y and z components of the current are zero everywhere.

Similarly, the total magnetic fields due to the y and z components of the current are

$$\mathbf{B}_2(\mathbf{r}') = \int_V (\mathbf{j}J_y(\mathbf{r})) \times \mathbf{H}(\mathbf{r}' - \mathbf{r}) dV \quad (38)$$

and

$$\mathbf{B}_3(\mathbf{r}') = \int_V (\mathbf{k}J_z(\mathbf{r})) \times \mathbf{H}(\mathbf{r}' - \mathbf{r}) dV \quad (39)$$

respectively. Therefore the total magnetic field due to all the three current components is

$$\mathbf{B}(\mathbf{r}') = \mathbf{B}_1(\mathbf{r}') + \mathbf{B}_2(\mathbf{r}') + \mathbf{B}_3(\mathbf{r}') \quad (40)$$

Let

$$\mathbf{B}(\mathbf{r}') = \mathbf{i}B_x(\mathbf{r}') + \mathbf{j}B_y(\mathbf{r}') + \mathbf{k}B_z(\mathbf{r}') \quad (41)$$

It can be expressed as

$$\mathbf{B}(\mathbf{r}') = \int_V \mathbf{J}(\mathbf{r}) \times \mathbf{H}(\mathbf{r}' - \mathbf{r}) dV \quad (42)$$

or

$$B_x(\mathbf{r}') = \int_V (J_y(\mathbf{r}) H_z(\mathbf{r}' - \mathbf{r}) - J_z(\mathbf{r}) H_y(\mathbf{r}' - \mathbf{r})) dV \quad (43)$$

$$B_y(\mathbf{r}') = \int_V (J_z(\mathbf{r}) H_x(\mathbf{r}' - \mathbf{r}) - J_x(\mathbf{r}) H_z(\mathbf{r}' - \mathbf{r})) dV \quad (44)$$

$$B_z(\mathbf{r}') = \int_V (J_x(\mathbf{r}) H_y(\mathbf{r}' - \mathbf{r}) - J_y(\mathbf{r}) H_x(\mathbf{r}' - \mathbf{r})) dV \quad (45)$$

The equations above have the form of a convolution expression which can be solved along with additional constraints for  $\mathbf{J}(\mathbf{r})$  in the Fourier domain. For example, representing respective Fourier transforms by lower case letters, and denoting spatial Fourier frequencies as,

$$\mathbf{u} = (u_x, u_y, u_z) = \mathbf{i}u_x + \mathbf{j}u_y + \mathbf{k}u_z \quad (46)$$

we obtain:

$$b_x(\mathbf{u}) = j_y(\mathbf{u}) h_z(\mathbf{u}) - j_z(\mathbf{u}) h_y(\mathbf{u}) \quad (47)$$

$$b_y(\mathbf{u}) = j_z(\mathbf{u}) h_x(\mathbf{u}) - j_x(\mathbf{u}) h_z(\mathbf{u}) \quad (48)$$

$$b_z(\mathbf{u}) = j_x(\mathbf{u}) h_y(\mathbf{u}) - j_y(\mathbf{u}) h_x(\mathbf{u}) \quad (49)$$

In matrix form, we may write the above equation as

$$\mathbf{b}(\mathbf{u}) \equiv \mathbf{H}'(\mathbf{u}) \mathbf{j}(\mathbf{u}) = \mathbf{j}(\mathbf{u}) \times \mathbf{h}(\mathbf{u}) \quad (50)$$

where

$$\mathbf{b}(\mathbf{u}) \equiv \begin{bmatrix} b_x(\mathbf{u}) \\ b_y(\mathbf{u}) \\ b_z(\mathbf{u}) \end{bmatrix} = \mathbf{i}b_x(\mathbf{u}) + \mathbf{j}b_y(\mathbf{u}) + \mathbf{k}b_z(\mathbf{u}) \quad (51)$$

$$\mathbf{H}'(\mathbf{u}) = \begin{bmatrix} 0 & h_z(\mathbf{u}) & -h_y(\mathbf{u}) \\ -h_z(\mathbf{u}) & 0 & h_x(\mathbf{u}) \\ h_y(\mathbf{u}) & -h_x(\mathbf{u}) & 0 \end{bmatrix} \quad (52)$$

$$\mathbf{j}(\mathbf{u}) \equiv \begin{bmatrix} j_x(\mathbf{u}) \\ j_y(\mathbf{u}) \\ j_z(\mathbf{u}) \end{bmatrix} = \mathbf{i}j_x(\mathbf{u}) + \mathbf{j}j_y(\mathbf{u}) + \mathbf{k}j_z(\mathbf{u}) \quad (53)$$

$$\mathbf{h}(\mathbf{u}) \equiv \begin{bmatrix} h_x(\mathbf{u}) \\ h_y(\mathbf{u}) \\ h_z(\mathbf{u}) \end{bmatrix} = \mathbf{i}h_x(\mathbf{u}) + \mathbf{j}h_y(\mathbf{u}) + \mathbf{k}h_z(\mathbf{u}) \quad (54)$$

The matrix/vector equation

$$\mathbf{b}(\mathbf{u}) = \mathbf{H}'(\mathbf{u}) \mathbf{j}(\mathbf{u}) = \mathbf{j}(\mathbf{u}) \times \mathbf{h}(\mathbf{u}) \quad (55)$$

is under-constrained and cannot be solved uniquely unless an additional constraint is employed. The determinant of  $\mathbf{H}'(\mathbf{u})$  can be verified to be zero. The additional constraint we can use is the Kirchoff's current law (or the applicable condition) at each voxel. The electric charge in a voxel is conserved and therefore the total charge or current flowing into any voxel from all neighboring voxels must be zero. In the discrete domain this condition can be expressed approximately for a voxel with dimensions  $\delta x \times \delta y \times \delta z$  by

$$J_x(\mathbf{r} + \mathbf{i} \delta x) - J_x(\mathbf{r} - \mathbf{i} \delta x) + J_y(\mathbf{r} + \mathbf{j} \delta y) - J_y(\mathbf{r} - \mathbf{j} \delta y) \quad (56)$$

$$+ J_z(\mathbf{r} + \mathbf{k} \delta z) - J_z(\mathbf{r} - \mathbf{k} \delta z) = 0$$

In the continuous domain, this condition can be expressed by

$$\text{Divergence of } \mathbf{J}(\mathbf{r}) = 0, \text{ or} \quad (57)$$

$$\nabla \cdot \mathbf{J}(\mathbf{r}) = \frac{\partial J_x(\mathbf{r})}{\partial x} + \frac{\partial J_y(\mathbf{r})}{\partial y} + \frac{\partial J_z(\mathbf{r})}{\partial z} = 0 \quad (58)$$

In the Fourier domain, the constraint Divergence of  $\mathbf{J}(\mathbf{r}) = 0$  becomes

$$(2\pi j)(u_x j_x(\mathbf{u}) + u_y j_y(\mathbf{u}) + u_z j_z(\mathbf{u})) = 0 \quad (59)$$

(Note:  $j$  in the above equation is the square root of -1).

The equation above can also be written as

$$\mathbf{u} \cdot \mathbf{j}(\mathbf{u}) = 0 \quad (60)$$

Using the above equation and the equation  $\mathbf{b}(\mathbf{u}) = \mathbf{H}'(\mathbf{u}) \mathbf{j}(\mathbf{u})$ , we can solve for

$j_x(\mathbf{u}), j_y(\mathbf{u}), j_z(\mathbf{u})$  and therefore  $\mathbf{J}(\mathbf{r})$ . The solution is found to be

$$\mathbf{j}(\mathbf{u}) = \mathbf{H}(\mathbf{u}) \mathbf{b}(\mathbf{u}) = \frac{\mathbf{u} \times \mathbf{b}(\mathbf{u})}{\mathbf{u} \cdot \mathbf{h}(\mathbf{u})}, \quad (61)$$

where

$$\mathbf{H}(\mathbf{u}) = \frac{1}{\mathbf{u} \cdot \mathbf{h}(\mathbf{u})} \begin{bmatrix} 0 & -u_z & u_y \\ u_z & 0 & -u_x \\ -u_y & u_x & 0 \end{bmatrix} \quad (62)$$

and

$$\mathbf{u} \cdot \mathbf{h}(\mathbf{u}) = u_x h_x(\mathbf{u}) + u_y h_y(\mathbf{u}) + u_z h_z(\mathbf{u}). \quad (63)$$

Inverse Fourier transform of  $\mathbf{j}(\mathbf{u})$  gives  $\mathbf{J}(\mathbf{r})$ . Thus a closed-form solution has been derived for the MEG problem. This same theory for MEG is also applicable to MCG. Equation (61) indicates that, in practice, a non-degenerate measured data set can be used to set up a linear system of equations and solved to obtain  $\mathbf{J}(\mathbf{r})$ .

#### Appendix D: Magnetic Density Imaging (MDI)

*[To be added later.]*

**Dr. Murali Subbarao** is a Professor of Electrical and Computer Engineering at Stony Brook University. His teaching and research interests are Computer Vision, Digital Image Processing, and 3D Medical Imaging. He obtained a B. Tech. degree in Electrical Engineering from the Indian Institute of Technology, Madras, and an M.S. and a Ph.D., both in Computer Science, from the University of Maryland at College Park. See [www.fieldparadigm.com](http://www.fieldparadigm.com) for more information. For two decades, he and his students developed an extensive theory of a computational approach to 3D machine vision for digital cameras. His approach was to carefully derive a detailed mathematical model for the forward image formation and sensing process, and use the model to derive algorithms for inverting the forward process. Now he has embarked on a similar mission to medical imaging devices such as SPECT/PET, MRI, ultra low-field MRI, and MEG. He has made significant progress and filed several patent applications.

*"We must see. We shall see."*